International Journal of Science and Research Archive
eISSN: 2582-8185
Cross Ref DOI: 10.30574/ijsra
Journal homepage: https://ijsra.net/

(RESEARCH ARTICLE)

Kalman filter design and flutter suppression control for an aeroelastic fin system

Mehmet Karahan [1, *] and Unver Kaynak [2]

[1] *TOBB University of Economics and Technology, Department of Electrical and Electronics Engineering, Sogutozu Caddesi No:43, 06510 Cankaya/Ankara, Turkiye.*
[2] *Turkish Aeronautical Association University, Aircraft Engineering, Bahcekapi, Okul Sk. No:11, 06790 Etimesgut/Ankara, Turkiye.*

International Journal of Science and Research Archive, 2026, 19(02), 489-500

Publication history: Received on 23 March 2026; revised on 04 May 2026; accepted on 07 May 2026

Article DOI: https://doi.org/10.30574/ijsra.2026.19.2.0957

Abstract

In aviation, flutter is a dangerous aeroelastic phenomenon resulting from uncontrolled, increasing vibration of structural parts such as wings or tails at high speeds due to aerodynamic forces, leading to a breakdown of structural integrity. This resonance-like condition is caused by the combination of the wing's bending and torsional modes. Uncontrolled flutter can quickly lead to structural damage in the wing and loss of function in the control surfaces. This can completely compromise flight safety. Therefore, flutter is one of the most important issues in international aircraft certification standards. In this research, an observer-based LQR control system was designed for active flutter suppression on a nonlinear two-degrees-of-freedom (2-DOF) aeroelastic wing model. Unmeasurable speed conditions were predicted in real-time using a Kalman filter, and a full state feedback control structure was obtained solely from sensor outputs. By examining different Kalman filter settings, the effects of measurement noise covariance on estimation accuracy and dynamic response speed were revealed. All modeling and simulation studies were performed using MATLAB/Simulink software.

Keywords: Flutter; Aeroelasticity; LQR control; Kalman filter; Modeling

1. Introduction

Aircraft wings can be subjected to dangerous vibrations called flutter as a result of the interaction of aerodynamic loads and structural flexibility [1]. When the flight speed exceeds a certain critical flutter speed, aerodynamic forces continuously feed the structural vibrations, rapidly increasing their amplitude [2]. Uncontrolled flutter can very quickly lead to structural damage in the wing, loss of function in control surfaces, and ultimately, a complete loss of flight safety [3]. Therefore, the flutter phenomenon is one of the most important issues examined in international aircraft certification standards [4].

Figure 1 shows the aeroelastic vibration modes and spatial distribution of these vibrations generated on the aircraft's wing and control surfaces during flutter; it reveals that the most critical deformations are concentrated in the wingtip and flap regions. Figure 1 represents the magnitudes of the complex-valued aeroelastic modes 9 and 8 [5].

* Corresponding author: Mehmet Karahan

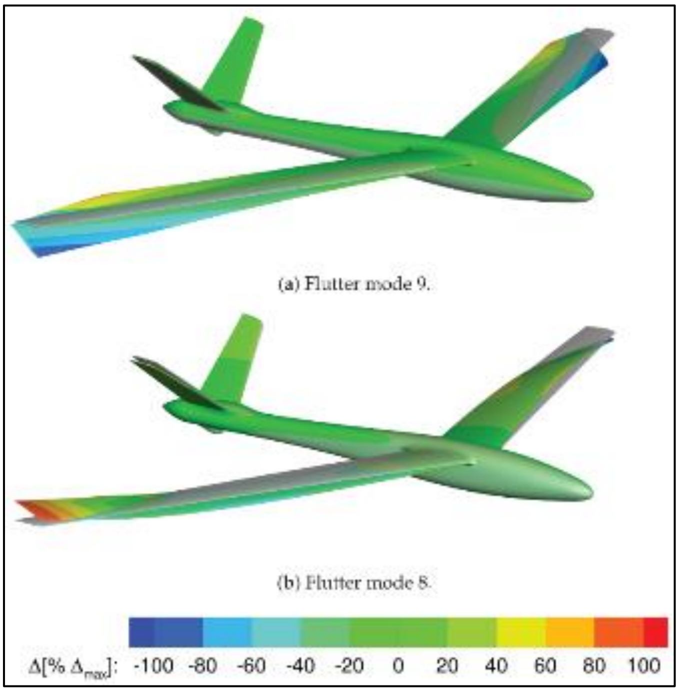

Figure 1 Displacement of the flutter modes [5]

In the past, passive methods such as making the wing more rigid, increasing structural mass, or changing the aerodynamic profile have been used to prevent flutter problems [6]. However, these methods have limitations such as increasing the weight of the aircraft, reducing fuel efficiency, and not providing sufficient performance in all flight conditions [7]. Today, since modern passenger aircraft (Boeing 787, Airbus A350, etc.) use lightweight and flexible composite wings, active flutter suppression systems have become critical [8]. Similarly, highly maneuverable fighter aircraft (F-16, F-35, etc.) are susceptible to flutter risk without active control because they fly at supersonic speeds with thin and flexible wing structures [9]. In this context, active flutter suppression systems have gained importance as an advanced technology at the intersection of aerodynamics, structural mechanics, and control engineering [10]. To ensure flight safety and prevent collisions, a robust design is necessary [11].

In this research, a control system for active flutter suppression was designed on a classical two-degrees-of-freedom (2-DOF) aeroelastic airfoil cross-section model. The model includes the pitch and plunge degrees of freedom of the wing. The control objective is to keep wing vibrations within safe amplitudes even under flight conditions above critical speed, i.e., to rapidly dampen flutter vibrations with active feedback. For this purpose, the system was modeled in the Simulink environment by adding nonlinear elements; flutter suppression was achieved by designing a Kalman state observer and an LQR state feedback controller around the resulting model. MATLAB/Simulink offers advantages such as ease of model analysis and a block diagram environment for dynamic system simulations [12]. Therefore, all modeling and simulation studies in this research were carried out using MATLAB/Simulink.

2. Materials and Methods

Figure 2 shows an aeroelastic wing cross-section model incorporating pitch-plunge movements. The free flow velocity U was chosen as 15 m/s, a value determined to ensure the system operates in the unstable flutter region. The air density is $\rho = 1.225$ kg/m^3. The damping and stiffness for the plunge motion are c_h and k_h. Damping and stiffness for the pitch motion are c_α and k_α. The cubic stiffening term representing nonlinear behavior is k_3. α represents the pitching angle.

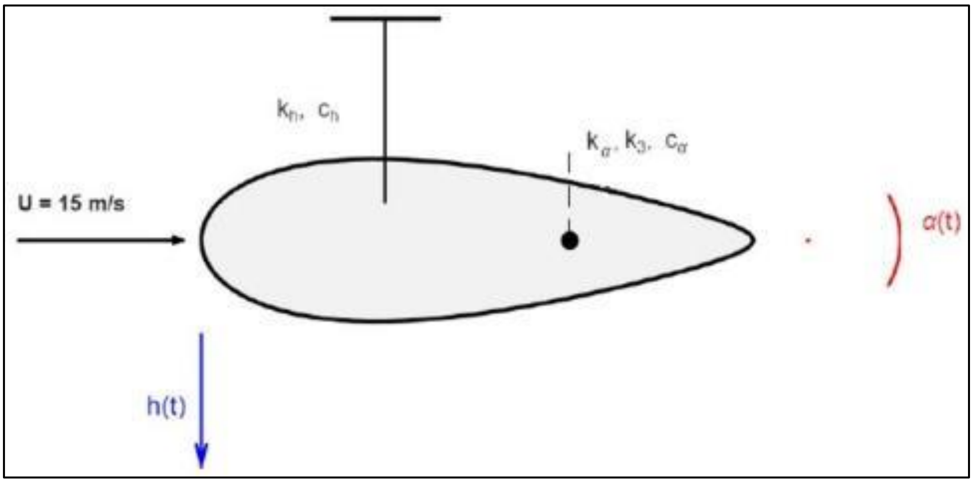

Figure 2 Aeroelastic wing cross-section model

The parameters for a two-degrees-of-freedom (bending and torsional) airfoil cross-section model used in aeroelasticity and flutter analyses are given in Table 1.

Table 1 The parameters for a 2 DOF airfoil cross-section model

Symbol	Definition	Value
m_s	Mass per unit span	12.38 kg/m
I_α	Moment of inertia of mass around the elastic axis	0.065 kg · m²/m
b	Wing half-chord length	0.135 m
x_α	Dimensionless static instability	0.2466
a	Position of the elastic axis	-0.4
c_h	Plunge damping coefficient	27.43 N · s /m
c_α	Pitch damping coefficient	0.036 N · m · s/rad
k_h	Plunge stiffness coefficient	2844.4 N/m
k_α	Pitch stiffness coefficient	3.525 N · m/rad
k_3	Cubic stiffness coefficient at the pitch degree	20
ρ	Standard air density at sea level	1.225 kg/m³
U	Free stream velocity	15 m/s
C_{la}	Lift curve slope	2π
C_{ma}	Static Pitch Stability	-0.5
$C_{l\beta}$	Side Force/Lift Effect	3
$C_{m\beta}$	Dihedral/Shear Moment Effect	-0.6

The system consists of a nonlinear aeroelastic wing model, sensors, a Kalman state observer, and an LQR-based feedback controller. Measured wing responses are subjected to state estimation using a Kalman filter, and the resulting state vector is fed to the LQR controller to ensure effective vibration suppression even at critical flutter speeds.

The state vector fed to the controller is not the actual states but the states ($\hat{x}$) estimated by the Kalman filter, and the LQR control law is applied based on these estimations. Furthermore, the flap angle command is applied to the nonlinear system by passing it through a saturation block representing the physical actuator limits.

In this study, a classical two-degrees-of-freedom (2-DOF) pitch-plunge airfoil cross-section model is used to represent the aeroelastic behavior. The overall coordinates of the system are as follows:

- $h(t)$: Up-down displacement of the airfoil relative to the rigid fuselage (plunge) in meters.
- $\alpha(t)$: Rotation angle of the airfoil relative to the aerodynamic axis (pitch) in radians.
- $\beta(t)$: Angle of the control surface (flap) in radians.

The state vector in this study is chosen as four-dimensional:

$$x(t) = \left[h(t), \dot{h}(t), \alpha(t), \dot{\alpha}(t)\right]^T \tag{1}$$

The system input is the angle change of the control surface (flap) located behind the wing:

$$\mathrm{u(t) = \beta(t)} \tag{2}$$

The outputs are chosen as the measurable quantities of the wing in equation (3). Thus, both displacement and pitch angle can be observed.

$$y(t) = \begin{bmatrix} h(t) \\ \alpha(t) \end{bmatrix} \tag{3}$$

The equations of motion of an aeroelastic system involve the interaction of the mass matrix (M), damping matrix (C), structural stiffness matrix (K) and aerodynamic forces. In general, in the linear case, they can be expressed as follows:

$$M\ddot{q}(t) + C\dot{q}(t) + K(q)q(t) = F_{aero} \tag{4}$$

Here, q(t) represents the free stream velocity.

$$q(t) = \begin{bmatrix} h(t) \\ \alpha(t) \end{bmatrix} \tag{5}$$

A two-degrees-of-freedom airfoil cross-section is typically defined as in equations (6) and (7). Here, (m) is the effective mass, I_a is the moment of inertia, and S_a is the coupling term arising from eccentricity.

$$M = \begin{bmatrix} m & S_a \\ S_a & I_a \end{bmatrix} \tag{6}$$

$$C = \begin{bmatrix} c_h & c_{ha} \\ c_{ah} & c_a \end{bmatrix} \tag{7}$$

In this study, a cubic spring term has been added to the pitch angle stiffness as a nonlinear effect on the model:

$$K(q) = \begin{bmatrix} k_h & 0 \\ 0 & k_1 + k_3 a^2(t) \end{bmatrix} \tag{8}$$

This means that the recovering moment of the pitch motion is modeled as in equation (9). This nonlinear term provides additional stiffness to the system, especially during large angular deflections, creating a realistic behavior.

$$M_{struct}(a) = \; k_1 a + k_3 a^3 \tag{9}$$

The aerodynamic loads are expressed as in equation (10) using a simplified version of a classical Theodorsen-based low-order model for constant speed (U). These loads include the lift force and aerodynamic moment components acting on the wing cross-section. The selected parameters were determined based on similar 2-DOF aeroelastic cross-section studies in the literature.

$$F_{aero} = \begin{bmatrix} L\left(h, a, \dot{h}, \dot{a}, \beta, U\right) \\ M\left(h, a, \dot{h}, \dot{a}, \beta, U\right) \end{bmatrix} \tag{10}$$

When the state vector for the four-state system is chosen as in equation (11), the nonlinear state-space equations can be written as in equation (12).

$$x_1 = h, x_2 = \dot{h}, x_3 = \alpha, x_4 = \dot{\alpha} \tag{11}$$

$$\dot{x}(t) = f\big(x(t), u(t)\big) \tag{12}$$

Here, the vector (f (·)) is obtained by appropriately rearranging the mass-damping-stiffness equations and aerodynamic loads given above. This expression was implemented numerically using the "Fcn/Matlab Function" blocks used after the integrator blocks in the Simulink model.

In this research, two separate Simulink models were created, separating the different analysis and control steps of the system. This simplified the numerical linearization step and made the overall system structure modular.

The linearized plant model represents only the physical part of the system, namely the two-degrees-of-freedom nonlinear aeroelastic wing system. It does not contain a controller or sensor model. Thanks to its simple structure, the system's A and B matrices were obtained numerically using MATLAB's linmod function. Figure 3 shows the plant model used for linearization.

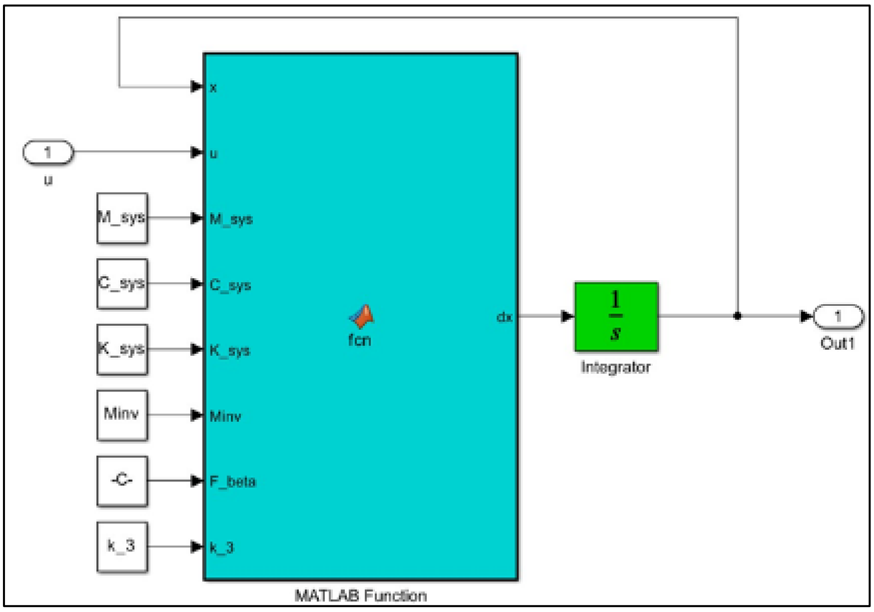

Figure 3 Linearized plant model

The basic characteristics of the model are given below.

- It only receives the flap control signal (β) as input.
- The outputs are the state variables h, α, ḣ and α̇.
- Since the nonlinear structure of the system is preserved, the linearization result obtained from this model is only valid around a certain equilibrium point.

The aim of this model is to obtain a linear approximation representing the behavior of a nonlinear aeroelastic system around small deflections, thereby enabling the derivation of suitable system matrices for Kalman filter and LQR controller design. The linear state-space model obtained as a result of the numerical linearization process is expressed as:

$$\dot{x}(t) = Ax(t) + Bu(t) \tag{13}$$

$$y(t) = Cx(t) + Du(t) \tag{14}$$

The matrices A, B, C, and D were transferred to the MATLAB workspace. This linear model was used as the basis for the design of the Kalman filter and LQR controller; the controlled behavior of the nonlinear system was evaluated through this approach.

The main model simulating the entire system behavior is a complete closed-loop system including the nonlinear physical system, the Kalman filter, and the LQR controller. The blocks it contains are shown in Figure 4.

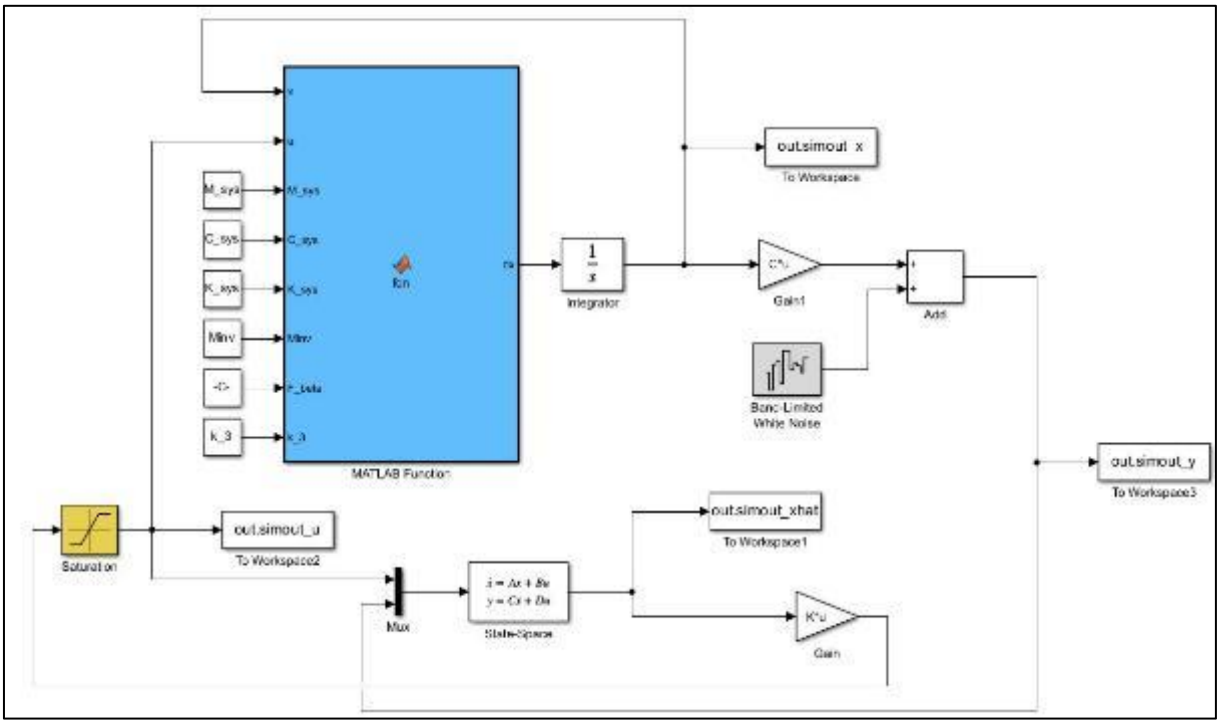

Figure 4 Main model

The components of the main system are as follows:

- Physical System (Plant): It has the same structure as the system in the linearized plant model.
- Kalman Filter: It is designed based on a linear system, which allows for the prediction of conditions despite sensor noise.
- LQR Controller: It is an optimal control approach designed to stabilize the system.
- Saturation: It includes a limiting block to prevent the flap angle from exceeding the physical limits of ±15°.
- Noise Inputs and Scenario Selector: It is prepared to compare the filter behavior with different Kalman parameters. White noise has been added to the output of the plant block to represent the actual sensor behavior.

Thus, the measurement signal fed into the Kalman filter is modeled as in equation (15), where v(t) is the zero-mean measurement noise with covariance R.

$$y_m(t) = y(t) + v(t) \tag{15}$$

The extended state-space model is given in equations (16) and (17).

$$\dot{x}(t) = Ax(t) + Bu(t) + w(t) \tag{16}$$

$$y_m(t) = Cx(t) + Du(t) + v(t) \tag{17}$$

All analyses, such as control performance, effects of different Kalman filter parameters, state estimation, and flap control, were performed based on this main model. The graphical results are also based on simulations in this model.

Since it is not possible to directly measure all state variables in the real system, a Kalman state observer was designed using a linear state-space model [13]. The Kalman filter estimates the system states in real time using the measurable outputs y(t) and the known control input [14]. In the filter design, model uncertainties and external effects are represented by process noise w(t), and sensor errors by measurement noise v(t); these noises are assumed to be zero-mean Gaussian processes [15]. Accordingly, process noise was modeled as w(t)~N(0, Q) and measurement noise as v(t)~N(0, R) [16].

For the linear model, the continuous-time Kalman filter gain matrix L was calculated using the lqe function in MATLAB and applied to the Kalman filter established in the Simulink model. The filter generates state estimations $\hat{x}(t)$ using the noisy measurement vector y_m (t) and control input β(t); these estimations are fed back to the LQR controller to provide closed-loop control. The performance of the Kalman filter was investigated by considering different values of the measurement noise covariance matrix R [17]. In the case of low R, the filter relies more on the measurements and follows the real system quickly, but some of the measurement noise is reflected in the prediction. In the case of high R, the prediction signal is smoother, but the behavior of the real system is followed with a delay, especially at the beginning and during sudden changes [18].

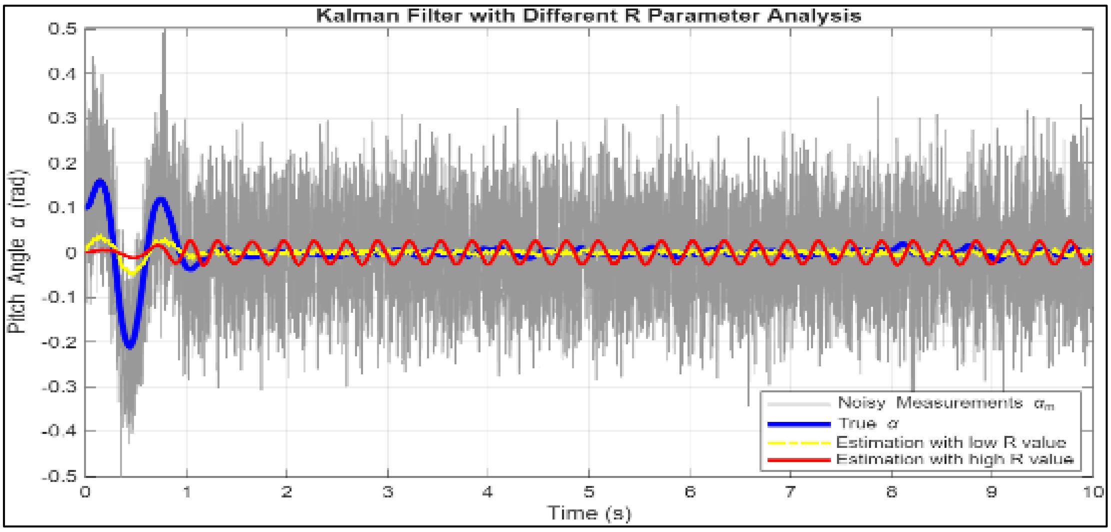

Figure 5 Kalman filter estimation with different R values for pitch angle

As shown in Figure 5, in the high R scenario, the filter relies more on the linearized model, resulting in insufficient representation of cubic hardening effects in the nonlinear system and leading to estimation delay. Due to the phase delay sensitivity of the flutter suppression problem, the low R scenario, which follows the real system faster, was found to be more suitable for control applications and was preferred in the remainder of the study.

A state feedback controller based on the Linear-Quadratic Regulator (LQR) method has been designed for the active control of the system. The LQR produces an optimal feedback gain by optimizing a specific performance index (cost function) on the linearized system model [19]. The aim of this study is to suppress flutter-like oscillations as quickly as possible while keeping the control surface movements as small as possible. In line with these objectives, the following continuous-time cost function has been defined:

$$\int_{0}^{\infty} \left(x^T(t) Q_{LQR} x(t) + u^T(t) R_{LQR} u(t) \right) dt \tag{18}$$

In equation (18), Q_{LQR} represents the weight given to the state, and R_{LQR} represents the weight given to the control input. In this study:

When designing the Q_{LQR} matrix, components representing vibration amplitudes, such as the wing's pitch angle α and plunge displacement h, were weighted with high coefficients. This increases the cost of deviations in these quantities, ensuring that when the system oscillates, the LQR controller will quickly attempt to bring them back to zero.

On the other hand, the R_{LQR} scalar coefficient was chosen to be large enough to prevent the flap control signal from becoming excessively amplified. This ensures that the controller will not generate disproportionately large control commands while attempting to dampen the vibration, keeping the flap angle within physical limits. Simulation tests showed that using larger pitching angle and velocity terms within the Q_{LQR} than larger plunge terms resulted in more effective suppression of the flutter mode. Finally, using the selected Q_{LQR} and R_{LQR}, the optimal feedback gain vector K was calculated in MATLAB using the lqr function.

This K matrix is defined in the linear model as in equation (19).

$$u = -Kx \tag{19}$$

Since not all states could be measured in the real system, the LQR control law was applied on the Simulink model based on the states estimated by the Kalman filter as in equation (20). This design forms a combined LQR + Kalman control structure.

$$u(t) = -K\hat{x}(t) \tag{20}$$

The flap angle command, which is the controller output, is restricted to the range of βmax = -15° and βmax = +15° according to equation (21) via the saturation block defined in Simulink.

$$\beta min \leq \beta(t) \leq \beta \mathrm{max} \tag{21}$$

Thus, even if the controller theoretically tries to generate a signal beyond these limits, the flap angle will not exceed the physical limits. This has enabled the control system to be tested under the actual actuator limits. Furthermore, the R_{LQR} coefficient has been chosen to ensure that the flap movements remain within the physical limits.

3. Results

The designed LQR controller and Kalman observer were integrated into a nonlinear aeroelastic system model, and various simulations were performed. At a constant flight speed U slightly above the critical flutter velocity, the system can remain in stable mode when the initial conditions are kept small around zero (because the linear system is in equilibrium around trim). To clearly observe the flutter phenomenon and test the effectiveness of the controller, the initial conditions were deliberately chosen to be large. Although the system response may be limited at small amplitudes due to nonlinear stiffening effects, it is observed that the system becomes unstable under larger deviations in the uncontrolled condition.

Figure 6 below shows the time-domain responses obtained for the pitch angle response of the system and the flap control input. The blue curves represent the results of the controlled state.

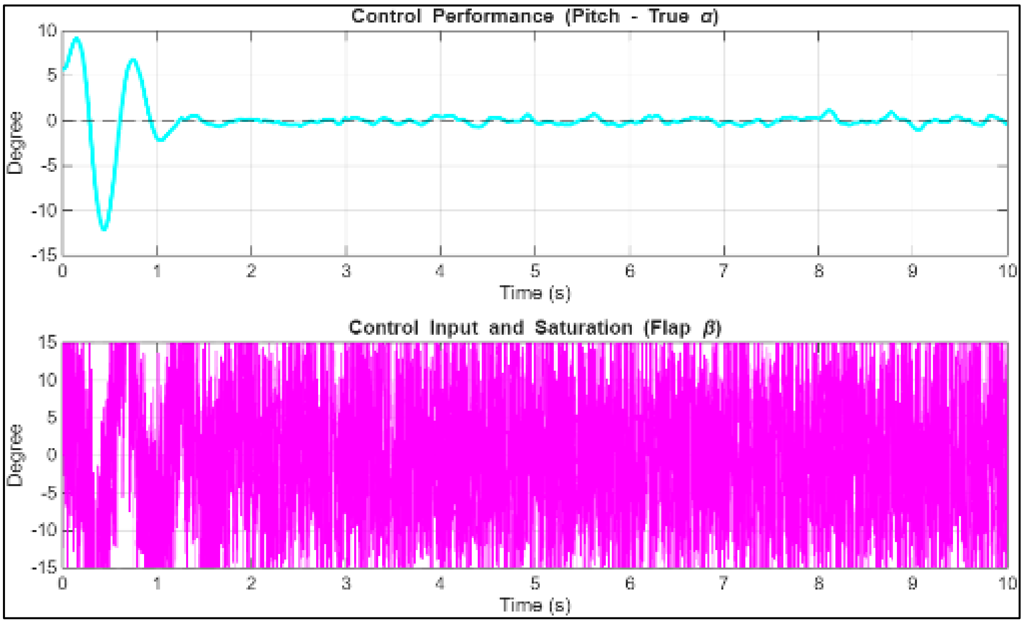

Figure 6 Control performance of the nonlinear system

The upper graph shows the change in the wing's pitch angle over time, in degrees. Initially, a large deviation of approximately 6 degrees is given for α_0 (zero-lift angle of attack). While this angular deviation would increase and lead to flutter drag if no control is applied, the vibration amplitude is rapidly reduced with LQR control. Around $t \approx 1$ s, the pitch angle has decreased to a small value around 0 degrees, meaning the settling time is approximately 1 second. Although there are small oscillations in the ± 0.5 degree range after $t > 1$ s due to small noise effects, these are acceptable and the system is kept in equilibrium.

The graph below shows the change in flap control input in degrees over time and the saturation limits. The controller commands the flap angle near its maximum limits to quickly correct the initial large error (drops at the ± 15 degree limit can be observed in the graph). At certain periods, the flap angle hits saturation (e.g., reaching the ± 15 degree level several times in the first second), but since the system calms down quickly, the flap command subsequently drops to fluctuations of the order of ± 5 degrees. This result indicates that the controller is operating under the physical actuator limits and that flap movements remain at a reasonable level.

Simulations have shown that the designed controller operates successfully in both linear and nonlinear models. The LQR gain designed around linearization was also able to dampen flutter vibrations in the actual nonlinear system. When comparing the controlled responses of the linear and nonlinear models, similar trends were observed except for minor differences; nonlinear effects did not lead to a significant degradation in performance. This confirms the validity of the modeling and design approach used. Furthermore, despite the added measurement noise, the feedback signal remained reliable thanks to the Kalman filter, and the control performance was not negatively affected.

The phase plane plot in Figure 7 visualizes the system's path from initial deflection to equilibrium. The trajectories plotted in the pitch angle–angular velocity phase space reveal the controller's effectiveness in flutter suppression from another perspective:

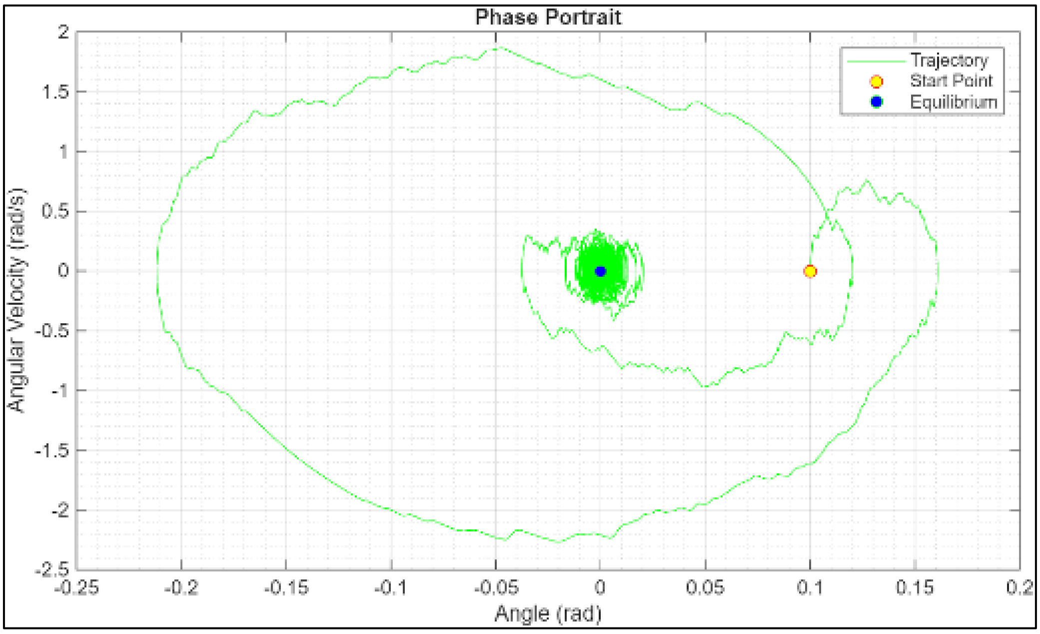

Figure 7 Phase portrait of the controlled system

The horizontal axis represents the pitch angle (in radians), the vertical axis represents the pitch angular velocity (in radians/s), and the green curve shows the state-space trajectory of the system over time. The yellow dot represents the initial state corresponding to a high initial deviation (e.g., alpha(0) ≈ 0.1 rad ≈ 5.7 degrees, alpha dot(0) is correspondingly high). Although the green trajectory initially traces an outward loop from this point (alpha has increased further due to the energy initially supplied to the system, reaching approximately 0.15 rad), the trajectory begins to narrow after the LQR control is activated. The curve is seen to spiral inward and shrink. Finally, the blue dot shows the equilibrium point of the system (alpha = 0, alpha dot = 0). The green trajectory gradually accumulates around the blue dot, meaning the system reaches a stable equilibrium. This phase portrait clearly demonstrates that the control system can dampen vibrations and maintain its equilibrium position even with large initial deviations. Considering that, in the absence of control, the system would follow an outward spiral in this phase space (unstable focus behavior), it is clear that the flight remained in a safe zone thanks to active flutter suppression. In particular, thanks to the appropriate selection of Kalman filter parameters, reliable status information was provided to the LQR controller even under measurement noise; this played a decisive role in the continuity of active flutter suppression performance.

4. Conclusion

This research presents the design and successful testing of an observer-based control system for active flutter suppression on a nonlinear two-degree-of-freedom (2-DOF) aeroelastic wing model. Unmeasurable velocity states are predicted in real-time using a Kalman filter, and a full state feedback control structure is obtained solely from sensor outputs. By examining different Kalman filter settings, the effects of measurement noise covariance on prediction accuracy and dynamic response speed are revealed.

The LQR controller, designed on a linearized model, demonstrated effective performance even on a nonlinear system; by selecting appropriate weighting matrices, the system was stabilized even under flight conditions exceeding the critical speed. The design objectives of settling time under 1 second and flap angle of ± 15° were met throughout all simulations.

According to the results obtained, under active control:

- Wing vibration amplitudes were significantly reduced and flutter-induced amplitude was completely suppressed.
- Unstable aeroelastic modes were damped by the feedback effect.
- The system maintained its stability despite nonlinear effects and sensor noise; the control structure was observed to be robust against model uncertainties.
- The controller output remained within the physical limits of the actuator, and the system did not lose stability even when the flap approached saturation.

In conclusion, the developed active flutter suppression system offers a successful solution for enhancing structural safety in critical flight conditions. It has been shown that aeroelastic instabilities, which cannot be effectively suppressed by passive methods, can be managed with modern control and observer-based approaches, as demonstrated in this study. The findings reveal that active flutter control strategies play a critical role in ensuring wing structural integrity and flight safety in both civil aircraft and highly maneuverable military platforms.

Compliance with ethical standards

Disclosure of conflict of interest

The authors state no conflict of interest.

References

[1] Basta, E., Ghommem, M., & Emam, S. (2021). Flutter control and mitigation of limit cycle oscillations in aircraft wings using distributed vibration absorbers. Nonlinear Dynamics, 106(3), 1975-2003. https://doi.org/10.1007/s11071-021-06889-z

[2] Kholodar, D. B. (2023). Aircraft flutter and aerodynamic work. Journal of Aircraft, 60(1), 56-65. https://doi.org/10.2514/1.C036846

[3] Karahan, M. (2025). Development Stages of Quadrotors from Past to Present: A Review. Drones, 9(12), 840. https://doi.org/10.3390/drones9120840

[4] Antimirova, E., Jung, J., Zhang, Z., Machuca, A., & Gu, G. X. (2024). Overview of computational methods to predict flutter in aircraft. Journal of Applied Mechanics, 91(5), 050801. https://doi.org/10.1115/1.4064324

[5] Rozov, V., Volmering, A., Hermanutz, A., Hornung, M., & Breitsamter, C. (2019). CFD- based aeroelastic sensitivity study of a low-speed flutter demonstrator. Aerospace, 6(3), 30. https://doi.org/10.3390/aerospace6030030

[6] Chai, Y., Gao, W., Ankay, B., Li, F., & Zhang, C. (2021). Aeroelastic analysis and flutter control of wings and panels: a review. International Journal of Mechanical System Dynamics, 1(1), 5-34. https://doi.org/10.1002/msd2.12015

[7] Kretov, A., & Tiniakov, D. (2022). Evaluation of the mass and aerodynamic efficiency of a high aspect ratio wing for prospective passenger aircraft. Aerospace, 9(9), 497. https://doi.org/10.3390/aerospace9090497

[8] Yazik, M. H. M., & Ismail, I. (2025). Aerospace structures and engines from polymer composites. In Aerospace Materials (pp. 349-383). Elsevier. https://doi.org/10.1016/B978-0-443-22118-7.00015-4

[9] Kim, C., Ji, C., Koh, G., & Choi, N. (2023). Review on flight control law technologies of fighter jets for flying qualities. International Journal of Aeronautical and Space Sciences, 24(1), 209-236. https://doi.org/10.1007/s42405-022-00560-6

[10] Ricci, S., Toffol, F., De Gaspari, A., Marchetti, L., Fonte, F., Riccobene, L., ... & Morgansen, K. (2022). Wind tunnel system for active flutter suppression research: Overview and insights. AIAA Journal, 60(12), 6692-6714. https://doi.org/10.2514/1.J061985

[11] Karahan, M., & Kasnakoglu, C. (2021). Path planning and collision avoidance with artificial intelligence for a quadrotor UAV. In 2021 International Conference Automatics and Informatics (ICAI) (pp. 163-166), Varna, Bulgaria.

[12] Karahan, M., Kurt, H., & Kasnakoglu, C. (2022). Moving object detection and counting in traffic with gaussian mixture models and vehicle license plate recognition with prewitt method. In 2022 International Symposium on Multidisciplinary Studies and Innovative Technologies (ISMSIT) (pp. 32-36), Ankara, Turkey.

[13] Afshar, S., Germ, F., & Morris, K. (2023). Extended Kalman Filter-Based Observer Design for Semilinear Infinite-Dimensional Systems. IEEE Transactions on Automatic Control, 69(6), https://doi.org/10.1109/TAC.2023.3319341

[14] Impraimakis, M., & Smyth, A. W. (2022). An unscented Kalman filter method for real time input-parameter-state estimation. Mechanical Systems and Signal Processing, 162, 108026. https://doi.org/10.1016/j.ymssp.2021.108026

[15] Nikolic, J., Furgale, P., Melzer, A., & Siegwart, R. (2015). Maximum likelihood identification of inertial sensor noise model parameters. IEEE Sensors Journal, 16(1), 163-176. https://doi.org/10.1109/JSEN.2015.2476668

[16] Bavdekar, V. A., Deshpande, A. P., & Patwardhan, S. C. (2011). Identification of process and measurement noise covariance for state and parameter estimation using extended Kalman filter. Journal of Process control, 21(4), 585-601. https://doi.org/10.1016/j.jprocont.2011.01.001

[17] Yin, Z., Yang, J., Ma, Y., Wang, S., Chai, D., & Cui, H. (2023). A robust adaptive extended kalman filter based on an improved measurement noise covariance matrix for the monitoring and isolation of abnormal disturbances in GNSS/INS vehicle navigation. Remote Sensing, 15(17), 4125. https://doi.org/10.3390/rs15174125

[18] Khodarahmi, M., & Maihami, V. (2023). A review on Kalman filter models. Archives of Computational Methods in Engineering, 30(1), 727-747. https://doi.org/10.1007/s11831-022-09815-7

[19] Karahan, M. (2025) Modeling and LQR Feedback Control for an Active Suspension of a High-Speed Train. Mühendislik Bilimleri ve Araştırmaları Dergisi, 7(1), 83-92. https://doi.org/10.46387/bjesr.1639115